

# Chaos in the Hamiltonian mean field model

Francesco Ginelli,<sup>1,2</sup> Kazumasa A. Takeuchi,<sup>3,4</sup> Hugues Chaté,<sup>3</sup> Antonio Politi,<sup>5,2,6</sup> and Alessandro Torcini<sup>5,6,7</sup>

<sup>1</sup>*Istituto dei Sistemi Complessi, CNR, via dei Taurini 19, I-00185 Roma, Italy*

<sup>2</sup>*Institute for Complex Systems and Mathematical Biology, King's College,  
University of Aberdeen, Aberdeen AB24 3UE, United Kingdom*

<sup>3</sup>*Service de Physique de l'État Condensé, CEA . Saclay, F-91191 Gif-sur-yvette, France*

<sup>4</sup>*Department of Physics, The University of Tokyo, 7-3-1 Hongo, Bunkyo-ku, Tokyo 113-0033, Japan*

<sup>5</sup>*Istituto dei Sistemi Complessi, CNR, via Madonna del Piano 10, I-50019 Sesto Fiorentino, Italy*

<sup>6</sup>*Centro Interdipartimentale per lo Studio delle Dinamiche Complesse,  
via Sansone, 1 - I-50019 Sesto Fiorentino, Italy*

<sup>7</sup>*INFN Sez. Firenze, via Sansone, 1 - I-50019 Sesto Fiorentino, Italy*

(Dated: May 6, 2022)

We study the dynamical properties of the canonical ordered phase of the Hamiltonian mean-field (HMF) model, in which  $N$  particles, globally-coupled via pairwise attractive interactions, form a rotating cluster. Using a combination of numerical and analytical arguments, we first show that the largest Lyapunov exponent remains strictly positive in the infinite-size limit, converging to its asymptotic value with  $1/\ln N$  corrections. We then elucidate the scaling laws ruling the behavior of this asymptotic value in the critical region separating the ordered, clustered phase and the disordered phase present at high energy densities. We also show that the full spectrum of Lyapunov exponents consists of a bulk component converging to the (zero) value taken by a test oscillator forced by the mean field, plus subextensive bands of  $\mathcal{O}(\ln N)$  exponents taking finite values. We finally investigate the robustness of these results by studying a “2D” extension of the HMF model where each particle is endowed with 4 degrees of freedom, thus allowing the emergence of chaos at the level of single particle. Altogether, these results illustrate the subtle effects of global (or long-range) coupling, and the importance of the order in which the infinite-time and infinite-size limits are taken: for an infinite-size HMF system represented by the Vlasov equation, no chaos is present, while chaos exists and subsists for any finite system size.

PACS numbers: 05.45.-a, 05.45.Xt, 05.70.Ln, 05.90.+m

## I. INTRODUCTION

In the context of Hamiltonian systems with long-range interactions, the Hamiltonian mean-field (HMF) model introduced by Antoni and Ruffo in 1995 [1] became the main benchmark for the investigation of thermodynamic and dynamical properties of non-additive systems [2, 3]. The HMF model describes an ensemble of  $N$  particles moving on a circle, coupled by pairwise (sinusoidal) attractive interactions. Each particle can also be seen as a pendulum in a fluctuating potential, whose amplitude is determined self-consistently and corresponds to the magnetization [1]. Detailed studies of the HMF model have revealed unusual properties, such as ensemble inequivalence (associated with the occurrence of negative specific heat), long-lived quasi-stationary states, and anomalous diffusion [2, 3].

Here, we are interested in the dynamical properties of the standard (microcanonical) equilibrium phases. Below the critical energy  $U_c = 3/4$ , the HMF system has a finite magnetization (clustered phase), while above  $U_c$  the magnetization vanishes (homogeneous phase). The two regimes are separated by a second order canonical phase transition. Both in the limit  $U \rightarrow 0$  and  $U \rightarrow \infty$  the dynamics is integrable: in the former case, all particles are trapped in the (harmonic) bottom part of the potential well; in the latter, they move freely along the circle. At intermediate energies, the (nonlinear) microcanonical

dynamics of a finite system made of  $N$  particles is characterized by a spectrum of Lyapunov exponents (LEs)  $\{\lambda_i\}$  with  $i = 1, \dots, 2N$  and, due to the Hamiltonian structure,  $\lambda_i = -\lambda_{2N+1-i}$ .

The thermodynamic limit is, however, a rather intriguing subject. For  $N \rightarrow \infty$ , the mean field is constant and the evolution of each particle is equivalent to the motion of a standard pendulum in a constant gravitational field. Accordingly, no chaos but just periodic orbits can be generated. This straightforward theoretical prediction is consistent with numerical simulations in the homogeneous phase, where it is numerically observed [2, 4] that the maximal LE  $\lambda_1$  vanishes as  $N^{-1/3}$  (a result which can be easily explained by invoking arguments developed for products of random matrices [2, 5, 6]). In contrast, in the clustered phase, some numerical investigations suggest that  $\lambda_1$  remains finite in the infinite-size limit. These findings are consistent with a theoretical study by Firpo [7] based on a Riemannian approach, which predicts finite  $\lambda_1$  values below the transition. However, recently, Manos and Ruffo [8] claimed that the  $N^{-1/3}$  law in the homogeneous phase applies also at low energies, specifically for  $U < 0.2$ , while in the range of  $0.2 < U < U_c$  they are unable to decide whether the maximal LE vanishes or stays finite. Finally, a recent statistical-mechanical treatment suggests that the Lyapunov spectrum should always converge to zero, but cannot exclude the existence of an anomalous subextensive component of strictly pos-

itive LEs [9].

In this paper we revisit this issue of the existence and nature of chaos in the HMF model. The main part of this paper is a study of the largest LE which is split into two parts: (i) the analysis of finite-time LEs of a single oscillator in the fluctuating potential under the assumption of a negligible coupling in tangent space; (ii) a careful investigation of the effect of the tangent-space coupling. The former analysis is justified by the empirical observation that the first Lyapunov vector is localized and the fact that the influence of a given oscillator on the self-consistent mean field, which we call simply the coupling strength, decreases as  $1/N$ . We conclude that the single-oscillator LE (i.e., the mean of finite-time LEs) cannot be larger than  $1/\ln N$ , but we also observe that its fluctuations stay finite in the thermodynamic limit. These results are related to the existence of a homoclinic cycle connecting the top of the effective potential with itself. The following analysis of the coupling in tangent-space reveals that even if it is very small it induces a finite increase in the LE, which is proportional to the fluctuations of the single-oscillator LE. This phenomenon, that we call “coupling pressure”, is a manifestation of a strong sensitivity to coupling which generally arises in ensembles of identical weakly-coupled oscillators. It was first uncovered in two coupled identical oscillators, where it was shown that the maximum LE increases with coupling strength  $\varepsilon$  by an amount of order  $1/|\ln \varepsilon|$  [10]. The same effect was later found in higher dimensional systems [11–14]. In the context of globally-coupled systems, the coupling pressure is so drastic that it survives even though the coupling strength vanishes in the thermodynamic limit. We provide a quantitative explanation of the effect, by mapping the tangent-space evolution onto a stochastic model of sporadically-coupled diffusing particles (see Ref. [15] for a preliminary discussion). In the HMF model, the effect of the coupling pressure is particularly important, since it increases the value of the largest LE from zero to a finite number, i.e., it induces an instability in a model that would, otherwise, be non-chaotic. Altogether, we can summarize our results by stating that the infinite-size and the infinite-time limits do not commute: taking first the thermodynamic limit, the evidence of dynamical instabilities would be lost. An indirect confirmation of the theoretical approach comes from the localization of the Lyapunov vector, that is confirmed by our numerical simulations.

Our investigation of the largest LE in the ordered phase of the simple HMF model is completed by the study of a number of related points: first, we numerically study the largest LE in the vicinity of the critical energy value  $U_c$ . We find that  $\lambda_1$  goes to zero for  $U \rightarrow U_c$  from below and account for the observed scaling behavior.

Next we address the problem of the shape of the entire Lyapunov spectrum. We find that several exponents (in addition to the largest) stay positive, but their number is non-extensive (i.e., it grows slower than linearly with  $N$ ). The results are consistent with the theory in

Ref. [9] where it was predicted that “with measure one” the spectrum should be equal to zero.

Finally, we discuss a 2D generalization of the HMF model [16, 17], to test the general validity of our theoretical and numerical findings. In the 2D model, each oscillator is composed of four variables and thus can be chaotic without taking the coupling pressure into account. We find nevertheless the same size-dependence of the largest LE as in the standard HMF model. We also investigate the full Lyapunov spectrum in this case and argue to what extent the argument developed for the standard HMF can be extended here.

This paper is organized as follows: The HMF model is introduced in Sec. II, together with a careful discussion of its equilibrium properties. This is necessary to collect proper information on finite-size effects that is crucial for a correct development of our theoretical arguments. Section III is devoted to a critical discussion of the numerical results for different system sizes and different energy values. There, we illustrate some of the issues that hindered the interpretation of the numerical results. Section IV is devoted to a detailed characterization of the evolution in the tangent space of a single particle in a self-consistent mean field. In particular, we introduce a finite-time LE and discuss its dependence on the energy and the number of particles. The effect of the coupling is discussed in Sec. V, where we first introduce a simplified model and test the correctness of our solution. The application to the HMF model is analyzed in the second part of the section. The scaling of the largest LE at the transition energy  $U_c$  is derived in Sec. VI and compared with numerics. The structure of the Lyapunov spectra is analyzed in Sec. VII. In Sec. VIII we deal with the 2D generalization of the HMF model. A brief summary of the results and a discussion of open questions are finally reported in Sec. IX.

## II. THE HAMILTONIAN MEAN FIELD MODEL: EQUILIBRIUM RESULTS

The HMF model was derived from a one-dimensional self-gravitating model, by truncating the Fourier expansion of the gravitational potential to its first term [1]. It consists of  $N$  unit-mass particles that move on a circle under their mutual attraction. The dynamics of the  $N$  particles is ruled by the Hamiltonian

$$H = K + V \equiv \sum_{i=1}^N \frac{p_i^2}{2} + \frac{1}{2N} \sum_{i,j=1}^N [1 - \cos(\theta_i - \theta_j)], \quad (1)$$

where  $\theta_i$  and  $p_i$  denote particle positions (angles) and velocities. The resulting equations of motion write

$$\begin{aligned} \dot{\theta}_i &= p_i, \\ \dot{p}_i &= \frac{1}{N} \sum_j \sin(\theta_j - \theta_i) = M \sin(\phi - \theta_i), \end{aligned} \quad (2)$$

where  $M$  is the magnetization and  $\phi$  the associated phase, defined by

$$Me^{i\phi} = \frac{1}{N} \sum_j e^{i\theta_j}. \quad (3)$$

$M$  measures the degree of clusterization and plays the role of an order parameter [18]. Depending on the energy density  $U = H/N$ , the system can show two different thermodynamic phases, separated by a second-order transition: (i) the clustered, ordered phase, characterized by a finite magnetization (for  $U < U_c = 3/4$ ); (ii) the homogeneous phase, characterized by a vanishing magnetization (for  $U > U_c$ ). In the following, we limit ourselves to the clustered phase  $U \leq U_c$  ( $T \leq T_c$ ).

All the reported simulations have been performed within the microcanonical ensemble by implementing symplectic integration schemes, typically a 4-th order McLahlan-Atela algorithm [19] with integration time step  $dt = 0.05$  or  $0.1$ . This choice ensures an energy conservation with a relative precision of the order of  $10^{-10}$  to  $10^{-11}$ .

Initial phases and momenta have been typically drawn from the invariant equilibrium distribution discussed in the next subsection. We have also occasionally compared the results with those obtained for different choices of initial conditions, namely: (i) zero phases and a Gaussian distribution of the momenta; (ii) a uniform distribution of the phases and a Gaussian distribution of the momenta. A transient (typically  $5 \times 10^3 N$  time units) has been discarded, before starting the computation of any equilibrium quantity. Finally the typical transient time for the evolution in tangent space lies between  $4 \times 10^5$  and  $4 \times 10^6$  time units, while the typical integration time lies between  $4 \times 10^6$  and  $10^7$  time units.

### A. Equilibrium distribution of single oscillator energy

From the point of view of a single oscillator, the evolution equation in Eq. (2), at finite system sizes, is equivalent to that of a pendulum in a noisy environment, the noise being the result of the statistical fluctuations of the magnetization. In the thermodynamic limit,  $M$  and  $\phi$  are strictly constant and, as a result, the single oscillator energy

$$h_i = \frac{p_i^2}{2} + M[1 - \cos(\theta_i - \phi)] \equiv k_i + v_i \quad (4)$$

is strictly conserved. Notice that, in Eq. (4), the (arbitrary) zero level of the potential energy  $v_i$  is shifted by  $v_M = M - 1$  in order that the ground-state energy of the single oscillator is always zero for any value of the magnetization  $M$ . This is the convention adopted throughout the paper [20]. Note also that the total potential energy is not given by the sum of the single potential terms, but

it is equal to half of it, namely

$$V = \frac{1}{2} \sum_{i=1}^N (v_i - v_M), \quad (5)$$

the reason being that each term would otherwise be counted twice.

The equilibrium distribution of the single-oscillator energies is

$$P(h, T) = \int_0^\infty dp \int_0^\pi d\theta \times \delta \left[ h - \frac{p^2}{2} - M(1 - \cos \theta) \right] Q(p, \theta, T), \quad (6)$$

where  $Q(p, \theta, T)$  is the Gibbs-Boltzmann distribution

$$Q(p, \theta, T) = C \exp \left[ -\frac{p^2}{2T} - \frac{M}{T}(1 - \cos \theta) \right], \quad (7)$$

with a suitable normalization constant  $C$ , the unit Boltzmann constant, and the temperature  $T$  given by [1-3]

$$U = \frac{T}{2} + \frac{1}{2}(1 - M^2). \quad (8)$$

As a result, one finds that

$$P(h, T) = \frac{C}{\sqrt{2M}} \int_0^{y_0} \frac{e^{-h/T}}{\sqrt{y(h/M - y)(2 - y)}} dy, \quad (9)$$

where  $y_0 = h/M$  if  $h/M < 2$  and  $y_0 = 2$  otherwise. The integrand has two (integrable) square-root singularities at both ends of the integration interval for all energy values, except for  $h = 2M$ , in which case the singularity is hyperbolic, and this indicates a logarithmic divergence of the integral. Note that the divergence lies at the separatrix  $e_s$  of the single-particle effective Hamiltonian (4). This equilibrium energy distribution (9) is plotted in Fig. 1(a) for three different energy densities ( $U = 0.15, 0.2$  and  $0.5$ ).

### B. Magnetization

In this section we discuss the behavior of the magnetization in the clustered phase and at the critical energy  $U_c$  for finite  $N$ . For large but finite  $N$ , the magnetization is affected by statistical fluctuations and, as a result, the oscillator energies diffuse, albeit very slowly. Simple statistical arguments suggest that the absolute value of the magnetization  $M(t)$  fluctuates around its mean field value with an amplitude that should scale as  $1/\sqrt{N}$ . We numerically checked this conjecture by measuring the power spectrum  $S(f)$  of the magnetization  $M(t)$  for different system sizes. In Fig. 1(b), we see that most of the power is concentrated in a broad peak around  $f = 0.16$  (for  $U = 0.5$ ) and the peak power scales as  $1/N$ , in agreement with the  $1/\sqrt{N}$  amplitude of the

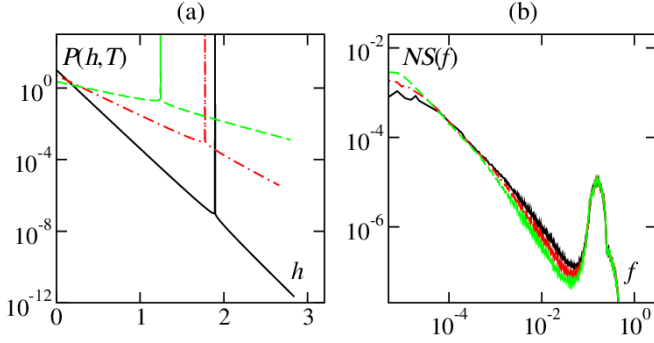


FIG. 1: (color online). (a) Equilibrium energy distribution [Eq. (9)] for three different values of the internal energy:  $U = 0.1$ ,  $U = 0.2$ , and  $U = 0.5$  (from bottom to top). The value of  $T$  in Eq. (9) is computed by Eq. (8). Recall the shifted energy axis, Eq. (4), for  $h$ . (b) Power spectrum  $S(f)$ , multiplied by the size  $N$ , for  $U = 0.5$  and three different system sizes,  $N = 250$  (solid black line), 500 (dotted dashed red line), and 1000 (dashed green line).

fluctuations. We also verified that the power contained in the low-frequency peak increases upon increasing the system size.

In contrast, the motion of the global phase is determined by the oscillators with single-particle energies  $h$  larger than the separatrix energy  $e_s$  [1]. They continue rotating either clockwise or counterclockwise according to their momentum  $p$ . The slow energy diffusion of individual oscillators implies that those with low energies wander and can reach  $h > e_s$ , “randomly” picking the rotation direction, and stay in this high-energy state for some time until they eventually go back to the “bounded” state with  $h < e_s$ . The numbers of particles rotating clockwise and counterclockwise are on average equal to one another, but, because of statistical fluctuations, the instantaneous fractions of the populations typically differ by a quantity of order  $1/\sqrt{N}$ . Because of momentum conservation, the phase  $\phi_N$  [21] of the global magnetization exhibits a net drift with an average angular velocity  $\omega \sim 1/\sqrt{N}$  [1], which has also been verified numerically (not shown). Over long time scales, the sign of the velocity changes since the fluctuations will invert the predominance of clockwise/counterclockwise rotating particles. As a consequence, we expect the global phase to exhibit a crossover from drifting to diffusive motion over a crossover timescale  $\tau_{\text{diff}}$ . Numerical simulations (see Fig. 2) clearly show that the crossover time diverges in the thermodynamic limit as  $\tau_{\text{diff}} \sim N$ .

Finally, we discuss the equilibrium behavior in proximity of the critical energy. In the thermodynamic limit, the magnetization  $M$  obeys the usual mean-field behavior, i.e.,  $M \sim |U - U_c|^{1/2}$  for  $U < U_c$  [2, 3]. Determining  $M$  for finite  $N$  is, however, a delicate problem which requires a careful treatment of finite-size fluctuations [22–24]. The correct solution can be found by taking into account the law of large numbers in the self-consistency equation of the mean field argument. The magnetization

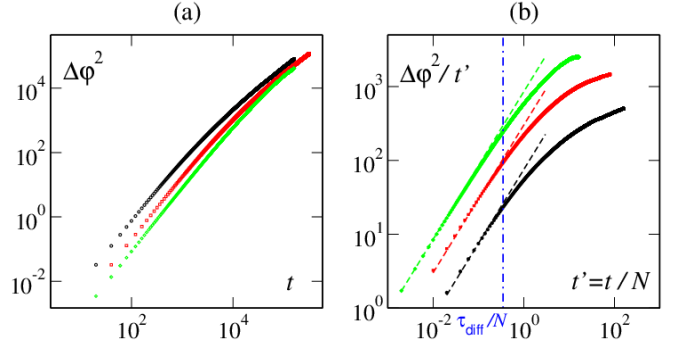


FIG. 2: (color online). (a) Mean-square displacement of the global magnetization phase  $\Delta\phi^2 = \langle (\phi(t) - \phi(0))^2 \rangle$  vs. time. Mean-square displacements have been computed by averaging over time span of order  $1 \times 10^7$  with sliding windows of duration 160000 – 320000 for three different system sizes: namely,  $N = 1000$  (black dots),  $N = 4000$  (red squares) and  $N = 10000$  (green diamonds). (b) Same quantities as in (a) but rescaled to better highlight the crossover from ballistic to diffusive behavior. Time has been rescaled by system size,  $t' = t/N$ , and mean-square displacements by the rescaled time,  $\Delta\phi^2 \rightarrow \Delta\phi^2/t'$ . The dashed lines mark the linear ballistic growth, and the vertical dot dashed (blue) line highlights the beginning of deviations from linear growth at the rescaled crossover time  $\tau_{\text{diff}}/N$ .

can be expressed within the canonical ensemble formulation as

$$M + \delta M = \left| \frac{1}{Z} \int_{-\infty}^{\infty} dp \int_0^{2\pi} d\theta e^{i\theta} e^{-\mathcal{H}/T} \right|, \quad (10)$$

where  $\mathcal{H} = p^2/2 + 1 - M \cos \theta$  (here the absolute scale is chosen for the energy),  $Z = \int_{-\infty}^{\infty} dp \int_0^{2\pi} d\theta e^{-\mathcal{H}/T}$ , and  $|\cdot|$  denotes the modulus of the complex number. The second term in the l.h.s. represents an unavoidable finite- $N$  correction that we assume to be in the order of  $\delta M \sim \mathcal{O}(M/\sqrt{N})$ . A straightforward calculation (see also Ref. [1]) leads to the self-consistency equation

$$M = \frac{I_1(M/T)}{I_0(M/T)} - \delta M, \quad (11)$$

where  $I_n(z)$  is the first-kind modified Bessel function of order  $n$ . Near the critical point, Eq. (11) can be expanded for small  $M$ , yielding

$$M \simeq \frac{1}{2} \frac{M}{T} \left[ 1 - \frac{1}{8} \left( \frac{M}{T} \right)^2 \right] - \delta M. \quad (12)$$

In the infinite size limit,  $\delta M = 0$ , and this gives the expected mean-field result [2, 3],  $M \sim (T_c - T)^{1/2}$  for  $T < T_c = 1/2$ . For finite sizes  $N$ , Eq. (12) predicts the following scaling,

$$M(U, N) \sim N^{-\beta/\nu} F((T_c - T)N^{1/\nu}), \quad \text{for } T < T_c, \quad (13)$$

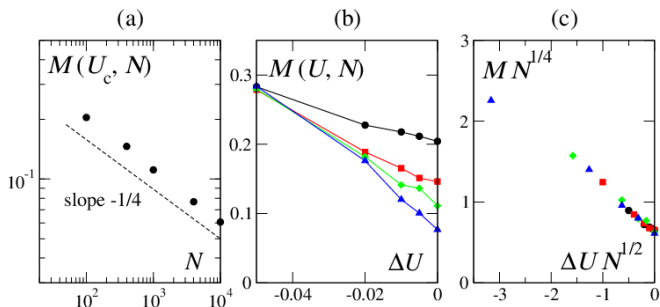


FIG. 3: (color online). Critical scaling of the magnetization  $M$ . (a) Size dependence of the magnetization at the critical point,  $M(U_c, N)$ . (b) Magnetization  $M(U, N)$  as a function of the energy difference  $\Delta U = U - U_c$  for  $N = 100, 400, 1000$ , and  $4000$  (from top to bottom). (c) Same data as the panel (b) with rescaled axes.

with  $\beta = 1/2$ ,  $\nu = 2$ , and a scaling function  $F(z)$ . Using the energy-temperature relation (8) [25], we can rewrite Eq. (13) as

$$M(U, N) \sim N^{-\beta/\nu} G\left((U_c - U)N^{1/\nu}\right), \quad \text{for } U < U_c, \quad (14)$$

with another scaling function  $G(z)$ . This expression accounts for the critical decay of the magnetization  $M(U_c, N) \sim N^{-1/4}$  found in Fig. 3(a). Equation (14) can be further checked by rescaling the magnetization  $M(U, N)$  off criticality; plotting  $MN^{\beta/\nu}$  against  $(U - U_c)N^{1/\nu}$ , we confirm that the data shown in Fig. 3(b) collapse reasonably well onto a single curve,  $G(z)$  [Fig. 3(c)]. It is worth noticing that the observed finite-size scaling  $M(U_c, N) \sim N^{-1/4}$  for the magnetization was reported for the first time for the mean field version of the Ising and Heisenberg model in Ref. [26]. The obtained value of the critical exponent  $\nu = 2$  is the one found for dissipative noisy phase oscillators [23], but is different from that of the Kuramoto model, i.e. deterministic phase oscillators with random frequencies,  $\nu = 5/2$  [24]. The value  $\nu = 2$  is also the one expected from a simple dimensional analysis,  $\nu = \nu_{\text{MF}} d_c$ , where  $\nu_{\text{MF}}$  is the usual correlation-length exponent in the mean-field limit and  $d_c$  is the upper critical dimension [27]. In our case,  $d_c = 4$  and  $\nu_{\text{MF}} = 1/2$ , which further confirms the analogy of the HMF model with the mean field XY Heisenberg model [1].

### III. LYAPUNOV CHARACTERIZATION OF THE DYNAMICS

In order to characterize the dynamics of the system, we estimate the LEs by following the dynamical evolution in tangent space of a vector  $\mathbf{v} = \{\delta\theta_i, \delta p_i\}_{i=1, \dots, N}$  of infinitesimal perturbations,

$$\begin{aligned} \delta\dot{\theta}_i &= \delta p_i, \\ \delta\dot{p}_i &= -M \cos(\phi - \theta_i) \delta\theta_i + \frac{1}{N} \sum_j \cos(\theta_j - \theta_i) \delta\theta_j, \end{aligned} \quad (15)$$

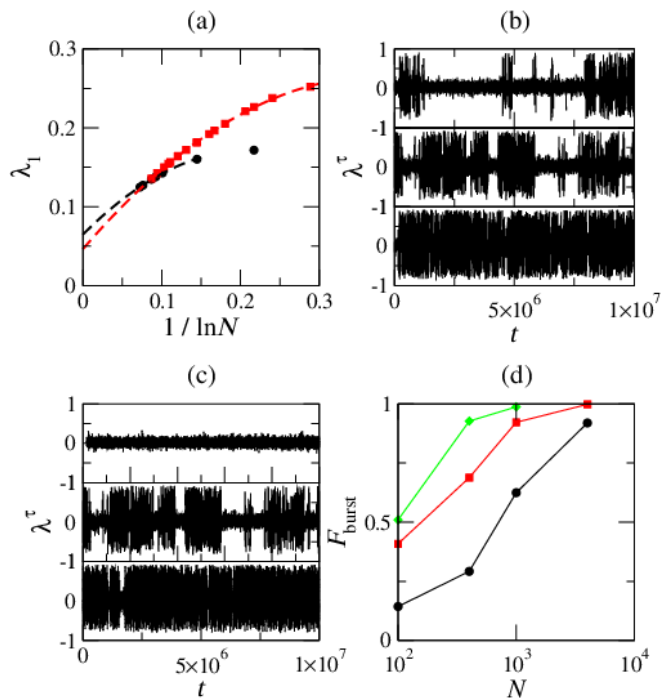


FIG. 4: (color online). Largest LE  $\lambda_1$  of the HMF model. (a)  $\lambda_1$  versus the system size  $N$  for  $U = 0.5$  (black circles) and  $U = 0.7$  (red squares). The dashed lines show the quadratic extrapolations to the asymptotic values. (b,c) Time series of the finite time exponent  $\lambda^\tau$  for  $N = 100, 400, 1000$  with  $U = 0.25$  (panel (b) from top to bottom) and for  $U = 0.20, 0.25, 0.30$  with  $N = 400$  (panel (c) from top to bottom). The laminar and burst states have different values of the time-averaged LE as shown in Fig. 6(c) below. (d) Time fraction in the burst state  $F_{\text{burst}}$  as a function of the size  $N$  for  $U = 0.25$  (black circles),  $0.30$  (red squares), and  $0.35$  (green diamonds).

and by orthonormalizing the resulting vectors at proper times [28]. In order to probe large system sizes up to  $N = 10^6$ , we have implemented a highly parallelized version of the Gram-Schmidt algorithm.

Most of the numerical simulations have been performed for  $U = 0.7$  (which corresponds to a magnetization  $M \approx 0.281$  and a temperature  $T \approx 0.479$ , measured at  $N \geq 10^5$ ) and  $U = 0.5$  ( $M \approx 0.621$  and  $T \approx 0.386$ ). Both parameter values are sufficiently away from the critical point  $U_c$  as well as from the zero-temperature limit; otherwise the asymptotic behavior of the Lyapunov exponent would be masked by severe finite-size effects (see below).

According to a theoretical argument briefly sketched in Ref. [15], where we showed that, in globally-coupled dissipative systems, the leading finite-size corrections to the asymptotic value of the largest LE are polynomial in  $1/\ln N$ , we find it convenient to investigate the finite-size dependence of  $\lambda_1$  by plotting it as a function of  $1/\ln N$ . The data reported in Fig. 4(a) are indeed consistent with

a logarithmic dependence,

$$\lambda_1 = \lambda_\infty + \frac{c}{\ln N} + \mathcal{O}\left(\frac{1}{\ln^2 N}\right), \quad (16)$$

for large  $N$ , especially for  $U = 0.7$  (red squares). Deviations from the  $1/\ln N$  behavior are visible for small  $N$ , but taking a quadratic correction into account is sufficient to describe perfectly all system sizes studied (Fig. 4(a), red dashed line). This quadratic correction is stronger for  $U = 0.5$ , which is an incipient evidence of the convergence problems that arise at small energies (see below). Because of this slow but significant size-dependence, the extrapolated values of the maximum LE in the thermodynamic limit are smaller than the typical values reported in the literature (see, e.g., Ref. [2]), but are nevertheless clearly different from zero:  $\lambda_\infty = 0.056(6)$  at  $U = 0.5$  and  $\lambda_\infty = 0.046(3)$  at  $U = 0.7$ , both obtained by using the quadratic ansatz described above.

As briefly mentioned in the introduction, a number of numerical studies have reported contradicting conclusions about the largest LE in the clustered phase: while most of them claimed, qualitatively, no or weak size-dependence and thus strictly positive asymptotic values of the maximal LE [2, 4], Manos and Ruffo [8] reported a power law decay  $\lambda \sim N^{-1/3}$ , although their simulations were performed for substantially lower energy densities ( $U = 0.1$ ). Our own numerical simulations (not shown) performed at  $U = 0.1$  indeed confirm the power-law decay at least up to  $N = 10^6$ . In order to shed some light on the possible existence of two qualitatively different phases, we scanned intermediate energy levels in the interval  $U \in (0.1, 0.5)$ . These simulations (see below) revealed the presence of strong intermittent behavior, which make practically impossible to determine a reliable value of the LE, in particular for large system sizes. The phenomenon is better illustrated by studying the finite time LE

$$\lambda^\tau(t) = \frac{1}{\tau} \ln \frac{\|\mathbf{v}(t)\|}{\|\mathbf{v}(t - \tau)\|}, \quad (17)$$

fixing  $\tau = 2$  [29]. Fig. 4(b,c) reveals irregular jumps of  $\lambda^\tau(t)$  between two clearly different states: (i) a *laminar* one, where  $\lambda^\tau(t)$  stays near zero; (ii) *bursts*, where  $\lambda^\tau(t)$  fluctuates much more strongly. Upon comparing simulations performed for different sizes [Fig. 4(b)] and different energy densities [Fig. 4(c)], we see that the frequency of the bursts grows both with  $N$  and  $U$ . This is quantitatively shown in Fig. 4(d).

In order to understand the origin of this intermittent behavior, we analyze the structure of the (first) Lyapunov vector. The Lyapunov vector is the quantity associated with each LE and indicates the direction of the infinitesimal perturbations growing at the rate of the corresponding LE. It is defined as a function of the phase-space point and turns out to be a useful tool to characterize statistical properties of large dynamical systems [30–32]. Here, it is convenient to introduce the squared amplitude

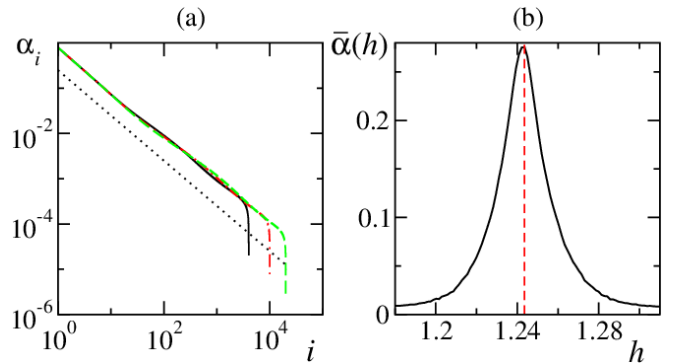


FIG. 5: (color online). Localization of the Lyapunov vector. (a)  $\alpha_i$  vs  $i$  for  $N = 4000$  (black solid line),  $N = 10000$  (red dotted dashed line), and  $N = 20000$  (green dashed line) at  $U = 0.5$ . The dotted black line marks a decay as  $1/i$ . (b) Average amplitude of the vector components as a function of the corresponding single-oscillator energy,  $\bar{\alpha}(h)$ , in a system of  $N = 10^5$  oscillators at  $U = 0.5$ . The vertical dashed red line marks the single oscillator separatrix energy  $e_s = 2M$ .

of the vector component for each oscillator,

$$A_i = \delta\theta_i^2 + \delta p_i^2, \quad (18)$$

and to consider its time average  $\langle A_i \rangle$  (here and in the following, angular brackets denote time averages), to have a statistically reliable quantity.

In homogeneous globally-coupled systems, any ordering of the oscillators is equally meaningful, as they are equivalent to one another. In Fig. 5(a), we plot the amplitude  $\alpha_i = \sqrt{\langle A_i \rangle}$  versus its rank (i.e., we arrange the oscillators according to  $\alpha_i$  in decreasing order) for  $N = 4000, 10000$ , and  $20000$ . Our data show that the Lyapunov vector is approximately localized as  $1/i$  (as indicated by the dotted black line), that is, the perturbation is concentrated in a few components. In Fig. 5(b), the data is organized in a different way. The oscillators are grouped according to their energy and the perturbation amplitude is averaged over all oscillators in the interval  $[h, h + dh]$ , to obtain  $\bar{\alpha}(h)$ . The results reported in Fig. 5(b) indicate that the vector component is substantially larger when the energy of the corresponding oscillator is close to that of the separatrix.

In order to further clarify the relationship between localization and energy, it is instructive to monitor the instantaneous degree of localization of the Lyapunov vector, by estimating the inverse participation ratio [33]

$$Y_2 = \frac{\sum_i A_i^2}{(\sum_i A_i)^2}. \quad (19)$$

By construction,  $1/N \leq Y_2 \leq 1$ . The larger is  $Y_2$ , the more the vector is localized;  $Y_2 = 1$  denotes complete localization on a single oscillator, while  $Y_2 = 1/N$  indicates a completely delocalized vector with equal components.

In Fig. 6(a), we plot the time evolution of the finite-time LE  $\lambda^\tau$ , of the inverse participation ratio  $Y_2$ , and of

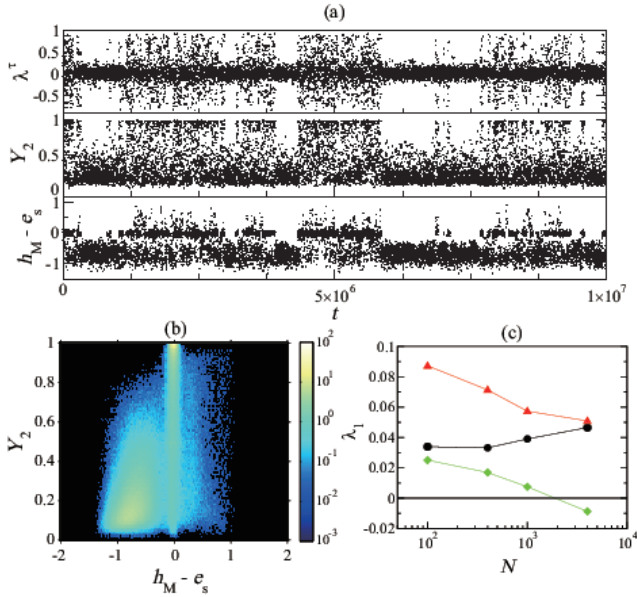


FIG. 6: (color online). Intermittency for  $U = 0.25$  and  $N = 400$ . (a) Time series of the finite-time LE  $\lambda^\tau$  (time window  $\tau = 2$ ), the instantaneous value  $Y_2$  of the inverse participation ratio, and the energy difference  $h_M - e_s$  between the dominating oscillator (the one with the largest amplitude  $A_i$  of the Lyapunov vector component) and the separatrix. (b) Density plot with respect to  $h_M - e_s$  and  $Y_2$ . The color code shows the frequency in the logarithmic scale. The black indicates null density. Two peaks corresponding to the burst and the non-burst states are clearly visible. (c) Lyapunov exponent  $\lambda_1$  (black circles) versus  $N$  for  $U = 0.25$ . The conditioned Lyapunov exponents (see text) are also shown for the burst state (red triangles) and for the non-burst state (green diamonds).

the energy  $h_M$  of the oscillator with the largest amplitude  $A_i$  in the Lyapunov vector components. The data refer to a small system ( $N = 400$ ) with energy density  $U = 0.25$ . The three temporal traces reveal a strong correlation between the occurrence of the bursts in the finite-time LE, a stronger localization and the closeness of the energy to that of the separatrix. A more quantitative characterization of the connection between the inverse participation ratio and the energy is presented in Fig. 6(b), where the color code indicates the probability to observe a given pair of values ( $Y_2, h_M - e_s$ ). Altogether, the data plotted in Fig. 6(a,b) confirm the intermittency between the two distinct states: (i) the laminar state is characterized by a less fluctuating finite-time LE, a weak localization of the Lyapunov vector, and single-oscillator energies far from the separatrix; (ii) the burst state by large fluctuations of the finite-time LE and a strong localization of the Lyapunov vector around an oscillator lying very close to the separatrix.

In Fig. 6(c) we compare the value of the true, time-averaged LE (circles) with the averages restricted to the bursts (triangles) and the laminar state (diamonds) for

$U = 0.25$ . We see that upon increasing the system size, the “burst” LE tends to converge towards the true LE. This reflects the fact that the laminar state tends to disappear for  $N \rightarrow \infty$  and the “laminar” LE remains quite small.

Therefore, we conclude this numerical analysis by noticing that the observed value of the LE depends strongly on whether there is at least one oscillator whose energy is sufficiently close to the energy  $e_s$  of the separatrix. If, for any reason, no oscillator has an energy  $h_i$  close enough to  $e_s$ , the laminar contribution dominates. Altogether, our analysis suggests that a truly asymptotic behavior is observed only if (on average) at least one oscillator has an energy sufficiently close to that of the separatrix. The minimal number  $N_m$  ensuring this condition can be estimated by imposing  $N_m P(e_s, T) \delta h = 1$  with a suitable width  $\delta h$  of the energy window. It grows quickly with decreasing  $U$ , since, for low energies, the energy distribution is approximately exponential,  $P(h, T) \approx \exp(-h/T)$  with  $T \approx 2U$  [see Eq. (8)], while the separatrix energy is practically constant,  $e_s = 2M \approx 2$ . By referring to the theoretical expression in Eq. (9) and assuming  $\delta h \approx 1/\sqrt{N}$  (see the next section for a justification), we find that  $N_m \approx 10^{13}$ ,  $10^5$ , and  $10$  for  $U = 0.1, 0.2$ , and  $0.5$ , respectively (these are the energy values considered in Fig. 1). It is clear that for  $U = 0.1$  there is no hope to reach the asymptotic regime in numerical simulations with the currently available machines and, in particular, that the  $\lambda_1 \sim N^{-1/3}$  scaling found by Manos and Ruffo [8] characterizes only the laminar state, which is not the asymptotic state of the system.

Although our numerical results strongly support the strictly positive asymptotic value of the maximal LE, it is not clear how this behavior is connected to the presence of oscillators in the vicinity of the separatrix. The following two sections are devoted to clarifying this point.

#### IV. SINGLE OSCILLATOR ANALYSIS

In this section we analyze the behavior of the Lyapunov exponent and vector, by neglecting the coupling term in the tangent space [i.e., the sum in Eq. (15)]. This assumption is tantamount to studying a single oscillator forced by the field  $M_N(t)e^{i\phi_N(t)}$ , which is generated self-consistently by an ensemble of  $N$  globally-coupled oscillators. The evolution is ruled by the effective Hamiltonian (4) and is thereby described by the equation

$$\begin{aligned} \dot{\theta} &= p \\ \dot{p} &= M_N \sin(\phi_N - \theta), \end{aligned} \quad (20)$$

which, in the tangent space, becomes

$$\begin{aligned} \delta\dot{\theta} &= \delta p \\ \delta\dot{p} &= -M_N \cos(\phi_N - \theta)\delta\theta. \end{aligned} \quad (21)$$

with no contribution from the coupling with the other oscillators. As already noted, the two observables  $M_N$

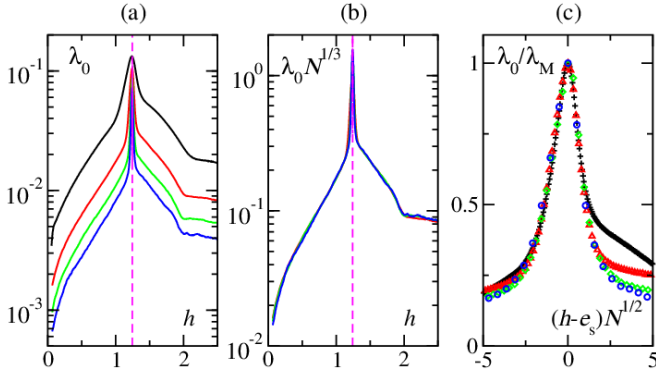


FIG. 7: (color online). Single-oscillator LE versus the energy of the single particle, forced by  $N$  globally-coupled oscillators at  $U = 0.5$ . In panel (a) the solid curves correspond to  $N = 100, 1000, 4000$ , and  $10000$  (from top to bottom); the three rescaled curves in panel (b) correspond to  $N = 1000, 4000$ , and  $10000$ . The curves overlap except in the peak region, or near the separatrix energy. The vertical dashed lines indicate the energy  $e_s$  of the separatrix. Panel (c) shows a close-up of the peak at  $h = e_s$ , the LE being scaled by the maximum value  $\lambda_M$  of each curve and plotted against rescaled single particle energies (crosses, triangles, diamonds, and circles correspond to  $N = 100, 1000, 4000$ , and  $10000$ , respectively).

and  $\phi_N$  are strictly constant in the thermodynamic limit  $N \rightarrow \infty$ . This means that the corresponding LE is expected to be equal to that of a standard pendulum, i.e., zero.

In the following, we investigate the size-dependence of the maximum LE of the single forced oscillator, by introducing an energy-dependent single-particle LE  $\lambda_0(h)$ . Since a meaningful definition of a LE involves the infinite-time limit, while energy is conserved only during finite times at finite  $N$ , we introduce sporadic small corrections to prevent the trajectory from diffusing away from the prefixed energy shell  $h$ . This is achieved by rescaling the kinetic energy, or the particle velocity, each time the trajectory passes through the point of minimal potential energy, without adjusting the potential energy.

The numerical results reported in Fig. 7 confirm that the LE decreases with increasing  $N$  as expected, but it also displays a strong dependence on the energy. The peak is centered at the energy  $e_s$  of the separatrix. In panel (b) we see that everywhere except in the peak area,  $\lambda_0$  scales as  $N^{-1/3}$ . This behavior can be understood by invoking known results for random symplectic matrices, similarly to the maximal LE of the full system in the homogeneous phase. It is known [34] that approximating the tangent-space dynamics with a product of independent symplectic random matrices with zero-mean disorder of amplitude  $\eta$  gives rise to a positive Lyapunov exponent which scales as  $\eta^{2/3}$ . In our setup, the statistical fluctuations of the collective magnetization scale as  $1/\sqrt{N}$  and play the role of the disorder. As a result,  $\eta \simeq 1/\sqrt{N}$  and this explains the  $-1/3$  scaling clearly seen in Fig. 7(b).

The same argument, however, does not apply to the oscillator with energy near  $e_s$ , because here the instability is rather due to the separatrix. This results in a peak in  $\lambda_0(h)$  at the separatrix energy, which does not decay as  $N^{-1/3}$ . We investigate the scaling behavior of its width, by plotting in Fig. 7(c) the LE normalized by its maximum value  $\lambda_M$  (for any given  $N$ ) with a rescaled axis  $(h - e_s)N^{1/2}$ . The nice overlap of the curves obtained at different system sizes shows that the width decreases as  $1/\sqrt{N}$ . This indicates that the anomalous behavior is exhibited by  $\mathcal{O}(\sqrt{N})$  oscillators located within the range of the separatrix energy. These are consequences of the  $\mathcal{O}(1/\sqrt{N})$  fluctuations of the magnetization.

Finally, in Fig. 8 we plotted  $\lambda_M$  for different values of  $N$  (see black squares). The data shows that  $\lambda_M$  scales as  $1/\ln N$  for large  $N$ . This behavior can be understood by introducing a suitable symbolic dynamics. The main source of uncertainty (and thus of entropy) is associated to the binary “choice” made by the oscillator on reaching the top of the potential, between the option to return to the same side or to pass it. Accordingly, we expect the metric entropy to be  $K \approx \ln 2/t_s$ , where  $t_s$  is the return time to the saddle [35]. The return time can be estimated as the time needed to amplify a distance from the saddle, in the order of the noise amplitude  $1/\sqrt{N}$ , to a value of order 1. Since the separation rate from the saddle is finite in the thermodynamic limit, the condition reads  $\exp(t_s)/\sqrt{N} \approx 1$ . Accordingly,  $t_s \approx \ln N$  and therefore  $K \approx 1/\ln N$ . Since the metric entropy is generically estimated by the sum of the positive LEs, which is simply equal to the sole positive LE in our case, we can finally conclude that  $\lambda_M \approx 1/\ln N$ , too. This prediction is confirmed in Fig. 8 with a quadratic correction for finite  $N$ , i.e.,  $\lambda_M \approx b_1/\ln N + b_2/(\ln N)^2 + \dots$ . Note that, in contrast to the first LE  $\lambda_1$  of the full system (red circles in Fig. 8),  $\lambda_M$  vanishes in the infinite-size limit as it should be (black squares). A similar argument can be used to infer asymptotic behavior of the fluctuations of the finite-time LE. Whenever the oscillator passes near the saddle, its growth rate is always of order 1, positive or negative, irrespective of the system size. This implies that the amplitude of the finite-time LE fluctuations near the separatrix energy should remain positive in the thermodynamic limit, possibly with logarithmic finite-size corrections.

By further comparing the single-oscillator LE  $\lambda_M$  with the first LE  $\lambda_1$  of the full system (see red circles in Fig. 8), we see that such a single oscillator contribution shows a size-dependence similar to that of the full-system LE. However, for increasing  $N$  there is no evidence that the gap is going to close. Indeed, Fig. 8(b) shows that  $\lambda_1 \ln N$  diverges for  $N \rightarrow \infty$ , suggesting that in the thermodynamic limit the relevant, non vanishing contribution to the first LE  $\lambda_1$  arises from the coupling terms. It is therefore necessary to consider more carefully the whole evolution equation in tangent space.

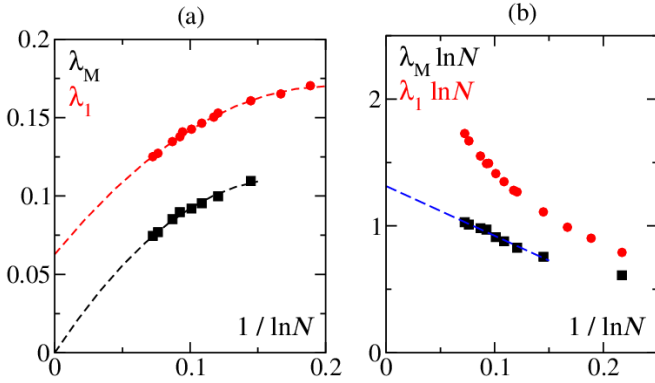


FIG. 8: (color online). Comparison between the maximum LE  $\lambda_M$  of a single forced oscillator (black squares) at separatrix energy  $e_s$  and the first LE  $\lambda_1$  of the full HMF model for  $U = 0.5$  (red circles). The dashed lines highlight the quadratic behavior  $\lambda_1, \lambda_M \sim b_0 + b_1/\ln N + b_2/(\ln N)^2$  with  $b_0 = 0$  for  $\lambda_M$ . (a) The LEs versus  $1/\ln N$ . (b) The LEs are multiplied by  $\ln N$ . The absence of the constant term  $b_0$  is confirmed by the linearly arranged symbols for  $\lambda_M$ .

## V. A SIMPLIFIED MODEL FOR THE COUPLING PRESSURE

In the context of globally-coupled dissipative systems, we recently showed that global coupling may induce an increase of the first LE with respect to the single-unit exponent [15]. Here, we refine such argument for the HMF context.

The single oscillator approximation discussed in the previous section consists in disregarding the contribution of the coupling term appearing in the second line of Eq. (15). In fact, as we explain below, this is what happens to the tangent-space evolution of the full system for most of the time, because of the localization of the Lyapunov vector (see Fig. 5) and the  $1/N$  normalization in front of the coupling term. The Lyapunov vector components then evolve independently. In particular, the logarithms of the amplitudes ( $x_i = \ln \sqrt{A_i}$ ) behave as Brownian particles with a drift velocity given by the single-particle LE and a diffusion constant that measures the fluctuations of the LE itself. The analysis carried out in the previous section suggests that the oscillators should be classified into two groups: (i) a small fraction which lies close to the separatrix and is characterized by a LE of order  $1/\ln N$ ; (ii) the vast majority, characterized by a LE of order  $N^{-1/3}$ . The  $\mathcal{O}(1/\sqrt{N})$  fluctuations of the magnetization then suggest that the population ratio between the particles close to the separatrix and the remaining population vanishes in the thermodynamic limit, possibly as  $1/\sqrt{N}$ . Moreover, energy diffusion induces (slow) exchanges between the two families.

We now discuss how the coupling modifies the single oscillator evolution. The localization of the Lyapunov vector indicates that the coupling term (the sum in the r.h.s. of Eq. (15)) is of the order of  $\delta\theta_m/N$ , where  $m$

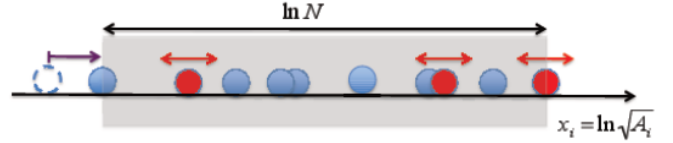


FIG. 9: (color online). Schematic representation of the toy model for the coupling pressure (see text). Point-like particles sit at the logarithmic coordinates  $x_i = \ln \sqrt{A_i}$  and are either diffusive (red circles) or non diffusive (blue). Diffusive particles turn non diffusive with a rate  $\alpha_1$  and non diffusive ones start to diffuse with a rate  $\alpha_2 \sim \alpha_1/\sqrt{N}$ , as the corresponding oscillators approach and leave the separatrix, respectively. The coupling is zero as long as particles are no farther than  $\ln N$  from the rightmost particle, but otherwise acts as a barrier, preventing particles from being farther than  $\ln N$  from the rightmost one. The net effect is a drift to the right.

labels the oscillator where the vector is localized. Therefore, because of the  $1/N$  factor, the  $m$ th oscillator component only weakly affects the oscillator at stake,  $\delta\theta_i$ , and so does the coupling term. However, the opposite is true when  $|\delta\theta_i| \ll |\delta\theta_m|/N$  (notice that this is possible, since the various components evolve independently of each other, and their logarithms diffuse away). In this latter case, the evolution is dominated by the coupling and the net result is that such extremely small components become of the order of the coupling term. In terms of the logarithmic coordinates  $x_i$ , the effect of the coupling can be schematized by a barrier sitting at  $x_{\min} = x_{\max} - \ln N$  (where  $x_{\max}$  labels the rightmost particle, that is the largest vector component) which prevents any interparticle distance from being larger than  $\ln N$ .

Altogether, we propose a simplified model of two populations of “particles”, as sketched in Fig. 9. The particles in the first group (red in Fig. 9) show the biased Brownian motion, while those in the other group (blue) stay quiescent. Each particle evolves independently of the others until it lies at a distance larger than  $\ln N$  to the left of the rightmost particle (where the Lyapunov vector is localized), in which case it is instantaneously pushed forward by the coupling to restore the maximal allowed distance (drawn by the gray box of size  $\ln N$  in Fig. 9). A precise formalization of the model requires the following additional ingredients: drift velocities and diffusion coefficients of the two populations and the mutual transition rates. For the drift, we assume that both populations are characterized by a zero velocity (zero LE). Since our goal is to explain the origin of a strictly positive LE in the thermodynamic limit, we believe that neither a  $1/N^{1/3}$  nor a  $1/\ln N$  LE can eventually provide a leading contribution and thereby set both to be zero. As for the diffusion coefficient of the Brownian particles, we assume a finite value  $D_s$  for the first population (that corresponding to the finite-time LE fluctuations of the oscillators in the vicinity of the separatrix). In contrast, we assume a zero diffusion coefficient for the second population, as it

is negligible for large sizes. As for the transition rates  $\alpha_1$  and  $\alpha_2$  from the diffusing to the still population and vice versa, respectively, on the basis of the numerical observation and the theoretical argument on the ratio of the two populations, we assume that the ratio  $\alpha_2/\alpha_1$  vanishes in the thermodynamic limit as  $1/\sqrt{N}$ . Thus, we are left with three independent parameters: the diffusion coefficient  $D_s$ , the transition rate from the diffusing to the still population  $\alpha_1$ , plus a small parameter  $\alpha_2$  of the order of  $\alpha_1/\sqrt{N}$ .

It is convenient to introduce the probability density  $P_j(x, t)$  for a particle of the  $j$ th population ( $j = 1$  and  $2$  referring to the diffusing and still populations, respectively) to be at position  $x$ . If both populations move with a positive velocity  $v$ , a positive LE spontaneously emerges in the system of interacting particles. It is convenient to study the problem in a frame moving with a velocity  $v$ , since then one has to look for a stationary solution. In this frame, the evolution equation reads,

$$\begin{aligned}\frac{\partial P_1}{\partial t} &= v \frac{\partial P_1}{\partial x} + \frac{D_s}{2} \frac{\partial^2 P_1}{\partial x^2} - \alpha_1 P_1 + \alpha_2 P_2, \\ \frac{\partial P_2}{\partial t} &= v \frac{\partial P_2}{\partial x} + \alpha_1 P_1 - \alpha_2 P_2,\end{aligned}\quad (22)$$

where  $x \in [0, \infty]$ , with a reflecting boundary at  $x = 0$ . Equation (22) describes an ensemble of stochastic particles that move along a tilted plane, which corresponds to the velocity  $v$  of the comoving frame, and have two possible internal states, one characterized by a finite diffusion  $D_s$  and the second one by a zero diffusion, so that the particles in the second state simply move toward the reflecting barrier at  $x = 0$ . The diffusive dynamics competes with the time scales set by the transition rates between the two populations. In particular, if  $D_s$  is finite and  $\alpha_1$  and  $\alpha_2$  are sufficiently small, particles in the non diffusing populations will tend to accumulate in  $x = 0$ . Therefore, we look for a general stationary solution of Eq. (22) of the form

$$\begin{aligned}P_1(x) &= c_1 e^{-\gamma x}, \\ P_2(x) &= c_0 \delta(x) + c_2 e^{-\gamma x},\end{aligned}\quad (23)$$

with some  $\gamma > 0$  and Dirac's delta  $\delta(x)$ . The two probability densities must obey particle conservation

$$\int_0^\infty (P_1(x) + P_2(x)) dx = 1, \quad (24)$$

and the population equilibrium condition

$$\alpha_1 \int_0^\infty P_1(x) dx = \alpha_2 \int_0^\infty P_2(x) dx. \quad (25)$$

Substituting the Ansatz (23) into Eq. (22), we obtain the stationary conditions in the bulk ( $x \neq 0$ ),

$$\begin{aligned}0 &= -v c_1 \gamma + \frac{D_s}{2} \gamma^2 c_1 - \alpha_1 c_1 + \alpha_2 c_2, \\ 0 &= -v c_2 \gamma + \alpha_1 c_1 - \alpha_2 c_2,\end{aligned}\quad (26)$$

which yields (for  $v \neq 0$ )

$$c_2 = c_1 \left( \frac{D_s \gamma}{2v} - 1 \right), \quad (27)$$

and

$$2\gamma v^2 + [2(\alpha_1 + \alpha_2) - D_s \gamma^2] v - D_s \alpha_2 \gamma = 0. \quad (28)$$

This can be solved for  $v$ , choosing the physically meaningful positive solution. By recalling that  $\alpha_2 \sim \alpha_1/\sqrt{N}$ , we can expand in terms of  $\alpha_2$ ,

$$v = \begin{cases} \frac{D_s \gamma}{2} - \frac{\alpha_1}{\gamma} + \mathcal{O}(\alpha_2) & \text{if } (\alpha_1 + \alpha_2) < D_s \gamma^2/2, \\ \frac{D_s \gamma}{2\alpha_1 - D_s \gamma^2} \alpha_2 - \mathcal{O}(\alpha_2^2) & \text{if } (\alpha_1 + \alpha_2) > D_s \gamma^2/2. \end{cases} \quad (29)$$

Note that the velocity (i.e., the LE) is strictly positive when diffusion dominates over the interstate transitions.

From Eqs. (23)-(25) it also follows

$$c_1 = \gamma \left( \frac{\alpha_2/\alpha_1}{1 + \alpha_2/\alpha_1} \right) \sim \gamma \frac{\alpha_2}{\alpha_1}, \quad (30)$$

and together with Eqs. (27) and (29), we find that the coefficient of Dirac's delta has a finite amplitude,

$$\frac{c_0}{2} = \begin{cases} 1 - \mathcal{O}(\alpha_2) & \text{if } (\alpha_1 + \alpha_2) < D_s \gamma^2/2, \\ \frac{D_s \gamma^2}{2\alpha_1} - \mathcal{O}(\alpha_2) & \text{if } (\alpha_1 + \alpha_2) > D_s \gamma^2/2. \end{cases} \quad (31)$$

We can now determine  $\gamma$  self-consistently. Given that we have an ensemble of  $N$  particles whose rightmost position is  $x_{\max} (= \ln N)$ , the integrated probability in the excess region,  $\int_{x_{\max}}^\infty (P_1(x) + P_2(x)) dx$ , should be in the order of  $1/N$ . From Eqs. (23) and (27) we have

$$e^{-\gamma x_{\max}} = \frac{2v}{D_s c_1} \frac{d_0}{N}, \quad (32)$$

where  $d_0$  is a constant of  $\mathcal{O}(1)$ . By substituting Eqs. (29) and (30) into Eq. (32) and using  $\alpha_2/\alpha_1 \sim 1/\sqrt{N}$ , we obtain, for small transition rates ( $\alpha_1 < D_s \gamma^2/2$ ),

$$e^{-\gamma x_{\max}} = \tilde{d}_0 \left( 1 - \frac{2\alpha_1}{D_s \gamma^2} \right) \frac{1}{\sqrt{N}} + \mathcal{O}(\alpha_2^2), \quad (33)$$

where  $\tilde{d}_0$  is another  $\mathcal{O}(1)$  constant.

In the HMF, the transition rate  $\alpha_1$  is the inverse of the residence time  $t_r$  of an oscillator near the separatrix energy, whose width has been shown to scale as  $1/\sqrt{N}$ . We now compute the scaling behavior of this residence time, analyzing more closely the dynamics near the energy maximum  $\theta - \phi_N = \pi$ . Consider a particle with energy  $2M_N$  and phase space coordinates  $p = 0$  and  $\theta = \phi_N + \pi$ . By expanding Eq. (4) around the potential energy maximum, we obtain

$$h \simeq \frac{p^2}{2} + 2M_N - \frac{M_N}{2} (\theta - \phi_N - \pi)^2 \quad (34)$$

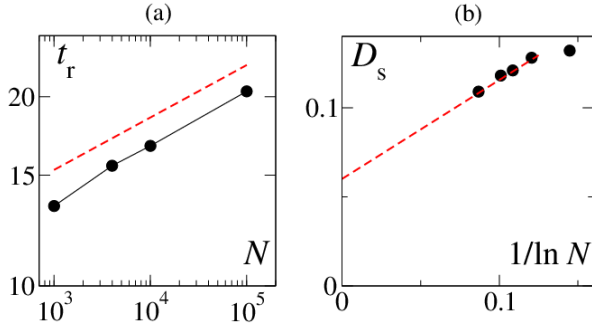


FIG. 10: (color online). (a) Average single-particle residence time  $t_r$  near the separatrix vs  $N$  for  $U = 0.5$ . The residence time is estimated by measuring the crossing time needed to a particle to pass from an energy  $e_L$  to an energy  $e_R$  or vice versa, where  $e_L < e_R$  are the two energies corresponding to the half maximum of the curve  $\lambda_0(h)$  reported in Fig. 7. The average is taken over  $5 \times 10^5$  to  $2 \times 10^6$  events for each size  $N$ . The dashed red line indicates  $N^{1/12}$ . (b) Diffusion coefficient  $D_s$  for a single forced oscillator at the separatrix energy (see text) as a function of  $1/\ln N$ . The plot highlights the finite size corrections of order  $1/\ln N$ . The red dashed line marks the linear extrapolation to the asymptotic value.

and the following equations for the single particle dynamics

$$\begin{aligned} \dot{\theta} &= p, \\ \dot{p} &\simeq M_N (\phi_N - \theta + \pi). \end{aligned} \quad (35)$$

We already know from Sec. II B that the global phase  $\phi_N$  exhibits a drift  $\Delta\phi = \phi_N(t) - \phi_N(0) \simeq \omega t$  on timescales smaller than  $\tau_{\text{diff}} \sim N$ . By integration, we find that  $\Delta\theta = \theta(t) - \theta(0) \sim \omega t^3$  which dominates the dynamics of the single particle energy for large times, as

$$\Delta h \sim \Delta\theta^2 \sim \omega^2 t^6. \quad (36)$$

By finally recalling that  $\omega \sim 1/\sqrt{N}$ , we can determine the scaling of the time needed for  $\Delta h$  to grow up to order  $1/\sqrt{N}$ , that is

$$\frac{1}{\alpha_1} = t_r \sim N^{1/12}, \quad (37)$$

which is in agreement with numerical results reported in Fig. 10(a).

As a result,  $\alpha_1$  goes to zero algebraically (albeit with a small exponent) in the thermodynamic limit and this guarantees that the inequality  $\alpha_1 < D_s \gamma^2/2$  is always satisfied asymptotically. By further imposing that  $x_{\text{max}}$  equals to the box width  $\ln N$ , we have from Eq. (33)

$$\gamma = \frac{1}{2} + \mathcal{O}\left(\frac{1}{\ln N}\right). \quad (38)$$

By now substituting Eq. (38) into Eq. (29), we finally obtain

$$v = \frac{D_s}{4} + \mathcal{O}\left(\frac{1}{\ln N}\right). \quad (39)$$

In other words, because of the divergence of the residence time near the separatrix, which induces sustained fluctuations of the finite-time LE, the asymptotic value of the velocity, or the (time-averaged) LE is finite. From the quantitative point of view, it is important to notice that our estimation for the asymptotic LE

$$\lambda_\infty = \frac{D_s}{4} \quad (40)$$

should be interpreted as a lower bound for the actual LE. In fact, it has been obtained by assuming the vanishing mean velocity for both of the populations, as well as the vanishing fluctuations for the still one. Accordingly, there are reasons to expect that the contribution to the LE from the coupling term may be larger than  $D_s/4$ .

In order to compare our estimate with the asymptotic value  $\lambda_\infty = 0.056(6)$  obtained at  $U = 0.5$  (see Sec. III), we estimated the diffusion coefficient  $D_s$  for a single forced oscillator lying at the separatrix energy  $h = e_s$ . Following the procedure outlined in Sec. IV, we computed the single-particle Lyapunov multiplier each time the trajectory passes through the point of minimal potential energy. From time series composed of  $\sim 10^6$  events, we estimate the associated mean-square displacement and thereby, assuming the standard linear diffusion, the corresponding diffusion coefficient  $D_s$ . The results are shown in Fig. 10(b). By varying the number  $N$  of forcing oscillators in the range  $10^3$  to  $10^5$  and choosing a logarithmic extrapolation, we obtained  $D_s = 0.06$ . Thus, it turns out that there is approximately a factor four difference between our estimate  $D_s/4$  and  $\lambda_\infty$ . The main interest of the formula (39) is that, by giving a lower bound, it proves that the largest LE should stay strictly positive in the infinite-size limit.

## VI. CRITICAL BEHAVIOR OF THE LARGEST LYAPUNOV EXPONENT

So far we have shown that, in the ordered phase  $U < U_c$ , the coupling pressure due to oscillators near the separatrix keeps the largest LE  $\lambda_1$  positive even in the infinite-size limit. This argument does not hold in the disordered phase  $U > U_c$ , where the magnetization  $M$  (and the separatrix) vanish. Instead, as already mentioned, the largest LE decays to zero as  $\lambda \sim N^{-1/3}$ .

An interesting question arises then quite naturally: what is the behavior of the largest LE in the vicinity of the critical point  $U_c$ ? The critical behavior of the largest LE  $\lambda$  may provide a connection between a dynamic quantity of the full system and macroscopic thermodynamic properties.

In this section we numerically investigate the critical properties of the largest LE  $\lambda_1(U, N)$  in the HMF model, providing a theoretical account for the observed finite-size scaling. We have already seen that, in the ordered phase,  $\lambda_1$  decreases logarithmically with increasing system size, toward a strictly positive asymptotic value

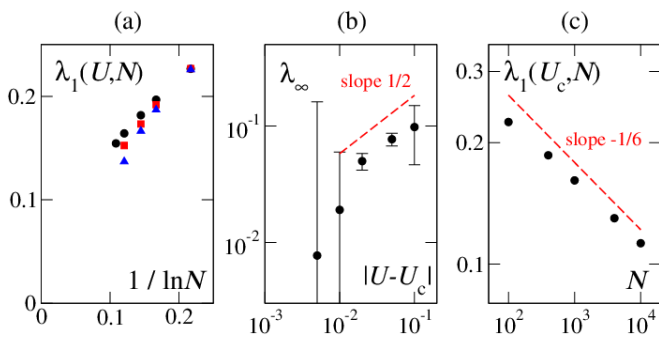


FIG. 11: (color online). Critical scaling of the largest LE  $\lambda_1(U, N)$ . (a)  $\lambda_1$  as a function of  $1/\ln N$  for different energies  $U = 0.70, 0.73$ , and  $0.745$  from top to bottom. (b) Extrapolated values of the asymptotic largest LE  $\lambda_\infty$  as a function of the distance from the criticality  $|U - U_c|$ . (c) Size dependence of  $\lambda_1$  at the critical point  $U = U_c$ .

$\lambda_\infty(U)$ . While approaching the critical point, however, we find that the logarithmic decay sets in at larger and larger sizes [Fig. 11(a)] and converges to smaller values of  $\lambda_\infty(U)$ . Although large finite-size effects as well as critical slowing down prevent us from estimating  $\lambda_\infty(U)$  near the critical point, our estimates in Fig. 11(b) suggest that the largest LE exhibits the same critical scaling as the magnetization with respect to the system energy  $U - U_c$ , namely,

$$\lambda_\infty(U) \sim |U - U_c|^{1/2}, \quad \text{for } U < U_c. \quad (41)$$

In this context Firpo's Riemannian theory [7] predicted a different power law  $\lambda_\infty(U) \sim |U - U_c|^{1/6}$  for  $U < U_c$ , though it was derived under assumptions that are not valid near the critical point.

At criticality, the logarithmic dependence of  $\lambda$  on  $N$  is replaced by an algebraic decay,  $\lambda_1(U_c, N) \sim N^{-1/6}$ , toward a vanishing  $\lambda_\infty$  [Fig. 11(c)]. In fact, this behavior can also be explained by the random matrix argument for the power-law decay  $\lambda_1 \sim N^{-1/3}$  in the disordered phase [2, 6]. In the latter case, the disorder of the matrices is due to the statistical fluctuations of the magnetization, and thus its amplitude  $\eta$  scales as  $1/\sqrt{N}$  and the largest LE  $\lambda_1 \sim \eta^{-2/3} \sim N^{-1/3}$ . By contrast, at the critical point, the disorder is due to the critical decay of the magnetization  $M(U_c, N) \sim N^{-\beta/\nu}$  (see Sec. II B), which yields

$$\lambda(U_c, N) \sim N^{-2\beta/3\nu}. \quad (42)$$

By recalling  $\beta = 1/2$  and  $\nu = 2$ , this indicates  $\lambda(U_c, N) \sim N^{-1/6}$ , in agreement with the numerical observation in Fig. 11(c).

## VII. THE FULL LYAPUNOV SPECTRUM

In this section we study the Lyapunov spectrum of the HMF model in the ordered phase. This analysis provides a more detailed characterization of the instability.

In particular it helps to assess the (non)extensivity of the chaotic dynamics. Given the difficulty of extending the theoretical arguments in Sec. V beyond the largest LE, we restrict our studies to a careful numerical analysis. Given the symmetry of the Lyapunov spectrum in Hamiltonian systems, it is sufficient to compute the first half.

In Ref. [8] it has been argued that, for  $U = 0.1$ , the full spectrum vanishes roughly as  $N^{-1/3}$ . However, the intermittent behavior observed at low energies [see, e.g., Fig. 4(b-d)] indicates that the burst state should eventually (for  $N$  large enough) dominate and thus the  $N^{-1/3}$  law eventually breaks down. Given this difficulty of dealing with low energy values, we focus here on a larger energy value, namely  $U = 0.7$ .

Figure 12(a) shows the Lyapunov spectra  $\lambda_i$  as functions of the rescaled index  $r \equiv (i - 0.5)/N$  for different system sizes  $N$ . This suggests that the spectrum is composed of two parts: the bulk of the spectrum which decays toward zero for increasing  $N$ , and the initial part pinned close to the largest LE, which is clearly visible in the inset of Fig. 12(a).

This scenario is actually coherent with the coexistence of extensive and subextensive chaos, recently discovered in generic globally-coupled dissipative systems [15]. In such systems, the Lyapunov spectrum is found to be asymptotically flat (a specific realization of extensivity) but sandwiched between two vanishing fractions of exponents located at both ends of the spectrum, where different asymptotic values appear. Finite-size analysis then revealed that the bulk of the spectrum scales as

$$\lambda_i \simeq \lambda_0 + \frac{c(r)}{\sqrt{N}} \quad (43)$$

where the asymptotic value  $\lambda_0$  corresponds to the LE of a single dynamic unit forced by the mean field [15].

In Fig. 12(b), one can appreciate that the spectrum of the HMF decays as predicted by Eq. (43) with  $\lambda_0 = 0$ , since a single oscillator has only two variables and thus cannot be chaotic. Notice that the existence of these zero-Lyapunov bulk components is consistent also with the theoretical prediction of Ref. [9], which did not exclude the presence of a vanishing (subextensive) fraction of different exponents. As for the power-law decay of the bulk exponents, the data for small  $r$ -values in Fig. 12(b) seem to decrease more slowly than  $1/\sqrt{N}$ , but this is presumably due to strong finite-size corrections induced by the bending near the beginning of the spectrum.

Concerning the subextensive LEs, in dissipative systems it was found that there are  $\mathcal{O}(\ln N)$  exponents whose values vary as  $\lambda^{(i)} \simeq \lambda_\infty + a(r')/\ln N + \mathcal{O}(\ln^2 N)$  with  $\lambda_\infty \neq \lambda_0$  independent of  $r'$ , when one fixes a logarithmically rescaled index  $r' \equiv (i - 1)/(i_0 + \ln N)$  with a constant  $i_0$  [15]. In the HMF, we have shown both numerical (Fig. 4) and theoretical (Sec. V) evidence of this logarithmic dependence for the largest LE,  $\lambda_1 \simeq \lambda_\infty + a(0)/\ln N + b(0)/\ln^2 N$ , with  $\lambda_\infty = 0.046(3)$

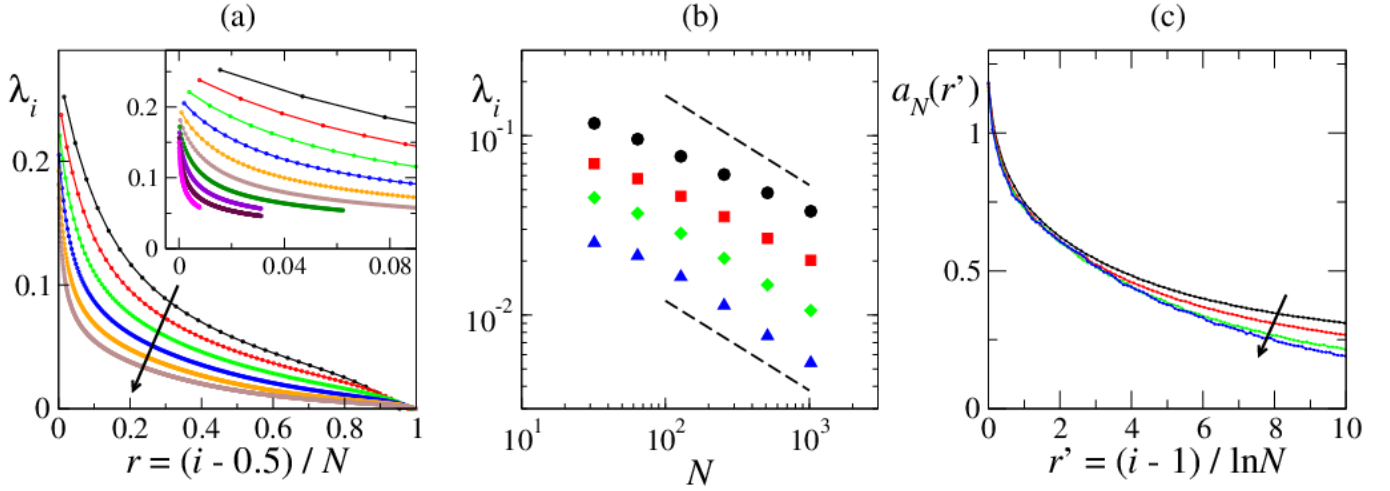


FIG. 12: Full Lyapunov spectrum at  $U = 0.7$ . (a) Lyapunov spectrum  $\lambda_i$  as a function of the rescaled index  $r \equiv (i - 0.5)/N$  for system sizes  $N = 32, 64, \dots, 1024$  from top right to bottom left, as indicated by the arrow. Inset: close-up of the first part, with sizes  $N = 2048, 4096, \dots, 16384$  added. (b)  $\lambda_i$  vs  $N$  at fixed rescaled indices  $h = 0.2, 0.4, 0.6$ , and  $0.8$  (from top to bottom). The dashed lines indicate  $\lambda_i \sim 1/\sqrt{N}$ . (c)  $a_N(r')$ , as defined in Eq. (45), plotted as a function of the logarithmically rescaled index  $r' = (i - 1)/\ln N$  for  $N = 1024, 2048, \dots, 16384$ . They show reasonable behavior toward the convergence, implying the logarithmic size-dependence (44) for these subextensive LEs (see text).

for  $U = 0.7$ . Now, we assume that the same size-dependence holds for subsequent LEs like in dissipative systems, with varying coefficients except for the constant term:

$$\lambda_i \simeq \lambda_\infty + a(r')/\ln N + b(r')/\ln^2 N. \quad (44)$$

To examine the validity of this expression, we take the Lyapunov spectra  $\lambda^{(N)}(r') \equiv \lambda_i^{(N)}$  at system size  $N$  and compute

$$a^{(N)}(r') \equiv \frac{\Delta\lambda^{(2N)}(r') \ln^2 2N - \Delta\lambda^{(N)}(r') \ln^2 N}{\ln 2}, \quad (45)$$

with  $\Delta\lambda^{(N)}(r') \equiv \lambda^{(N)}(r') - \lambda_\infty$ . If Eq. (44) holds, the definition in Eq. (45) gives  $a^{(N)}(r') \simeq a(r')$  and the size-dependence vanishes. Figure 12(c) tests this idea and indeed verifies that  $a^{(N)}(r')$  approaches an asymptotic curve for large sizes  $N$  with the logarithmically rescaled

index  $r' = (i - 1)/\ln N$  (here  $i_0$  is set to be zero). Therefore, the logarithmic size-dependence (44) holds for these subextensive exponents, similarly to dissipative systems. Although we need to study larger systems to obtain a firmer numerical support, our results on the full spectrum of the HMF model are consistent with the coexistence of extensive and subextensive exponents, previously found for dissipative systems.

## VIII. THE GENERALIZED HMF MODEL

In order to study the generality of our results, we finally turn our attention to a two-dimensional variant of the HMF model, introduced by Antoni and Torcini [17] and later generalized [2, 16] to the present form. It is defined by the Hamiltonian

$$H = \sum_{i=1}^N \frac{p_{x,i}^2 + p_{y,i}^2}{2} + \frac{1}{2N} \sum_{i,j=1}^N \{ [1 - \cos(x_i - x_j)] + [1 - \cos(y_i - y_j)] + A [1 - \cos(x_i - x_j) \cos(y_i - y_j)] \}, \quad (46)$$

with two-dimensional coordinates  $(x_i, y_i)$ , their conjugate momenta  $(p_{x,i}, p_{y,i})$ , and a coupling constant  $A$ . The equations of motion can be written as,

$$\begin{aligned}\dot{x}_i &= p_{x,i}, \\ \dot{y}_i &= p_{y,i}, \\ \dot{p}_{x,i} &= -M_x \sin(x_i - \phi_x) - \frac{A}{2} [P_+ \sin(x_i + y_i - \psi_+) + P_- \sin(x_i - y_i - \psi_-)], \\ \dot{p}_{y,i} &= -M_y \sin(y_i - \phi_y) - \frac{A}{2} [P_+ \sin(x_i + y_i - \psi_+) - P_- \sin(x_i - y_i - \psi_-)],\end{aligned}\quad (47)$$

with four mean field terms defined as

$$M_z e^{i\phi_z} \equiv \frac{1}{N} \sum_{i=1}^N e^{iz_i} \quad z = \{x, y\}, \quad P_{\pm} e^{i\psi_{\pm}} \equiv \frac{1}{N} \sum_{i=1}^N e^{i(x_i \pm y_i)}. \quad (48)$$

As a matter of fact, because of the symmetries of the model, on average  $M_x \sim M_y \sim M$  and  $P_+ \sim P_- \sim P$  and the model can be described in terms of two order parameters only.

This generalized HMF model is known for its rich and generic behavior within the class of systems with long-range interactions [2, 16, 17]. For  $A = 0$  it reduces to the standard HMF model [Eq. (1)]. More generally, while the standard HMF model shows a continuous transition from the homogeneous to the ferromagnetic, single-cluster phase, the generalized HMF model can exhibit both continuous and discontinuous canonical transitions depending on the value of  $A$ , as shown in its phase diagram (Fig. 13). Moreover, there exists another ordered phase, called hereafter the double-cluster phase, which is composed of two clusters of oscillators separated on average by  $\pi$  both in  $x_i$  and  $y_i$ , and thus characterized by finite values of  $P$  and a vanishing magnetization  $M$ . On the microscopic side, the essential difference with the standard HMF model is that here a single oscillator has four variables, and hence can be chaotic in the absence of any coupling with either an external field or other oscillators. The largest LE of the full system is therefore not purely determined by the coupling effect, unlike in the standard HMF model, but receives also a contribution from the local dynamics, which depends on the single-oscillator energy.

Figure 14(a) shows the largest LE  $\lambda_1$  measured for three different sets of parameter values:  $A = 0.2, U = 1.4$  (point  $P_1$  in Fig. 13), in the single-cluster phase, close to a (canonical) continuous transition [black circles in Fig. 14(a)];  $A = 1.0, U = 1.5$  (point  $P_2$ ), in the single-cluster phase, close to a (canonical) discontinuous transition (green diamonds); and  $A = 6.0, U = 5.0$  (point  $P_3$ ), in the double-cluster phase (red squares). In all the three cases, the largest LE shows the  $1/\ln N$  scaling toward nonzero asymptotic values, similarly to the standard HMF model. From the figure, one notices that in proximity of continuous transitions  $\lambda_1$  decreases with  $N$ , while at  $P_2$ , in proximity of the discontinuous transition, the maximal LE increases with the system size. This

peculiarity deserves further investigations.

Analogously to the 1D case, it is instructive to start comparing with the behavior of a single oscillator forced by constant order parameters. At variance with the 1D case, the resulting value of the LE can be positive here and depends on the energy. When one compares the extrapolated asymptotic values  $\lambda_{\infty}$  of the full-system LE with the maximum value of the single-oscillator LE,  $\lambda_s$ , over possible energy values, we obtain  $\lambda_{\infty} = 0.16$  and  $\lambda_s = 0.11$  at  $P_1$ ,  $\lambda_{\infty} = 0.38$  and  $\lambda_s = 0.27$  at  $P_2$ , and  $\lambda_{\infty} = 0.23$  and  $\lambda_s = 0$  at  $P_3$ ; the first asymptotic LE of the full system is systematically larger than  $\lambda_s$ . This is

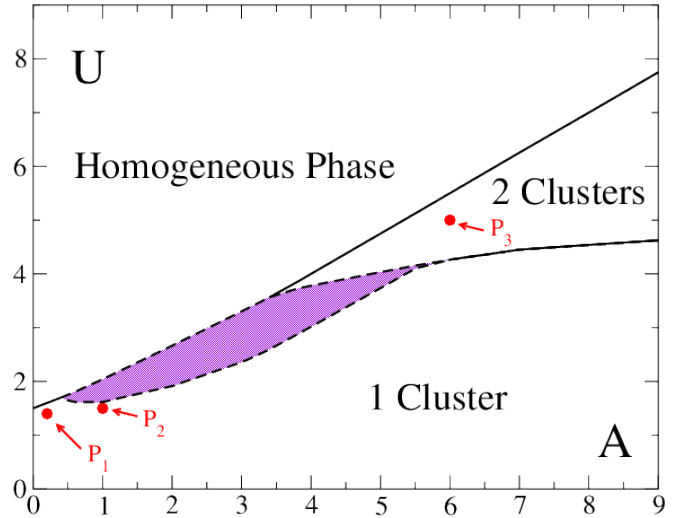


FIG. 13: (color online). Phase diagram of the generalized HMF model. The shaded area denotes the region where microcanonical and canonical ensembles differ from one another (i.e. the coexistence region of two different thermodynamic phases) occurring in correspondence of discontinuous canonical transitions. Solid and dashed lines correspond to continuous and discontinuous transitions, respectively, within the canonical ensemble. The red dots indicate the three parameter values we have studied.

again a manifestation of the coupling pressure discussed in Sec. V. For the first two cases, because of the chaotic dynamics of the single oscillator, one does not need to introduce the two-family approach taken for the standard HMF model, but it is more meaningful to refer to the treatment developed in Ref. [15] for dissipative systems, which predicts,

$$\lambda_\infty = \bar{\lambda}_s + \frac{D}{2} \quad (49)$$

where  $D$  is the diffusion coefficient for the fluctuations of the single-oscillator finite-time LE and  $\bar{\lambda}_s$  is the single-oscillator LE with an appropriate averaging over energy values. By taking into account this correction and using  $\lambda_s$  instead of  $\bar{\lambda}_s$  for the sake of simplicity, we find:  $\lambda_\infty \approx 0.18$  ( $D = 0.15$ ) at  $P_1$ , and  $\lambda_\infty \approx 0.33$  ( $D = 0.12$ ) at  $P_2$ . The new values are much closer to the extrapolated ones, though there is still a remaining gap (especially in the second case), which is presumably due to the fact that Eq. (49) was derived under the assumption of short ranged time correlations. The slow diffusion across different energy surfaces makes this assumption at least questionable. In contrast to these cases for the single-cluster phase, the situation in the double-cluster phase is rather analogous to the standard HMF model; because  $M = 0$  in the infinite-size limit, the equations of motion in this limit reduce to

$$\dot{p}_{x,i} \pm \dot{p}_{y,i} \simeq -AP \sin(x_i \pm y_i - \psi_\pm), \quad (50)$$

which are equivalent to two uncoupled standard HMF models [Eq. (2)]. However, our theoretical approach in Sec. V should not be applied directly to this case, because it deals with finite sizes, where the two variables in Eq. (50) are coupled in a non-trivial manner.

We also studied the full Lyapunov spectrum  $\lambda_i$  of the generalized HMF model. The results shown in Fig. 14(b) are obtained at  $P_2$ . They indicate that the full spectrum becomes flatter and flatter for larger sizes, with an apparent power-law decay of  $\lambda_i$  with fixed rescaled index  $r$  (inset). While the convergence toward zero was expected in the 1D case, this behavior is questionable for the 2D model because the single oscillator is not chaotic in the presence of a constant magnetization. In fact, it is reasonable to expect that, analogously to the dissipative mean-field models discussed in Ref [15], the exponents in the bulk of the spectrum converge to the value of the LE of a single forced oscillator without coupling in tangent space. However in a Hamiltonian model such as the 2D HMF, it is not clear which exponent one should refer to, as it depends on the energy and, moreover, the phase space is filled with stable islands. Direct measurement of the energy of a single oscillator in the full system of size  $N$  indicates that, within sufficiently long time scales, the single-oscillator energy diffuses as largely irrespective of  $N$  [Fig. 14(c)]. Given this existence of a well-defined distribution function  $\rho(h)$  for the single-oscillator energy, an appropriate reference value  $\bar{\lambda}_s$  for the single-oscillator

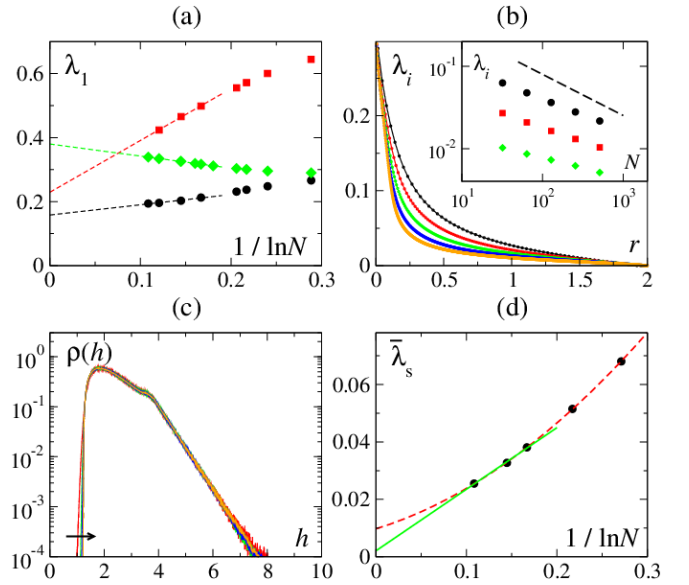


FIG. 14: (color online). Lyapunov exponents in the generalized HMF model. (a) Largest LE of the full system,  $\lambda_1$  vs  $1/\ln N$  for  $A = 0.2, U = 1.4$  (black circles);  $A = 1.0, U = 1.5$  (green diamonds); and  $A = 6.0, U = 5.0$  (red squares). The dashed lines indicate linear fits to the scaling regime. (b) Full spectrum  $\lambda_i$  vs  $r = (i-0.5)/N$  with  $N = 32, 64, 128, 256$ , and  $512$  (from top to bottom) for  $A = 1.0, U = 1.5$ . Inset:  $\lambda_i$  vs  $N$  for fixed rescaled indices  $r = 0.5, 1.0, 1.5$  from top to bottom. (c) Distribution of the single-oscillator energy  $h$  in the system of size  $N = 40, 100, 400, 1000$ , and  $4000$ . The arrow indicates increasing system size. (d) The LE  $\bar{\lambda}_s$  of a single oscillator forced by the full system of size  $N$ . The red dashed and green solid lines show the results of a linear and quadratic fitting, respectively, which result in finite asymptotic values of  $\bar{\lambda}_s$ .

LE would be simply the exponent averaged with this distribution function, namely,

$$\bar{\lambda}_s = \int dh \rho(h) \lambda_s(h) \quad (51)$$

where  $\lambda_s(h)$  is the energy-dependent single-oscillator LE. At finite  $N$ , this is nothing but the conventional time-averaged LE of a single forced oscillator and is reported in Fig. 14(d). This substantially decreases with increasing  $N$  and, in particular, in the infinite-size limit, it can reach a positive but quite small value in the order of  $10^{-3}$  [estimated by a linear fit in Fig. 14(d)]. This indicates that the decreasing bulk exponents reported in the inset of Fig. 14(b) can have such a small but positive asymptotic value, which is however indistinguishable from zero from the available numerical data. Moreover, one should notice that each oscillator has two nonnegative LEs; the first one can be positive or zero as already discussed, while the second one is always zero because of the continuous time. It implies that one may even expect the occurrence of two bands in the asymptotic bulk spectrum, in correspondence with these two single-oscillator LEs. Further studies are necessary to clarify these is-

sues, to elucidate the generality of the extensivity and subextensivity found for the standard HMF model.

## IX. CONCLUSIONS AND OPEN PROBLEMS

The question whether the largest LE in the HMF model remains positive or converges to zero in the thermodynamic limit has remained unsettled for a long time. We have shown here that the largest LE is indeed positive by making use of several subtle properties of globally-coupled systems. The first ingredient is what we call the “coupling pressure” which induces a finite increase in the largest LE (with respect to the LE of a single oscillator forced by the mean field). Coupling pressure is a general phenomenon that occurs in globally-coupled models of both dissipative and conservative dynamical systems and arises from the fluctuations of single-oscillator finite-time LEs. However, the 1D HMF dynamics is even more subtle, since the LE of the single oscillator under a constant field is strictly zero, and its relevant fluctuations must be computed by referring to a special type of trajectories that come close to the separatrix. More “natural” is the behavior of the 2D HMF, since the single oscillator dynamics is chaotic and thus the overall scenario is analogous to that of standard dissipative chaotic systems (see Ref. [15]). Altogether, our results indicate that the thermodynamic limit is rather singular. If one first takes the limit  $N \rightarrow \infty$ , no fluctuations can be expected and no signature of chaos detected. On the other hand, we have shown that the largest LE of an arbitrarily large system is always positive. This means that representations of the dynamics such as that built in the Vlasov equation (which corresponds to assuming  $N = \infty$ ) lose the chaoticity of the original dynamics captured by the largest LE.

On a more quantitative level, we have been able to derive an explicit expression for a lower bound of the largest LE. It would be interesting to improve the argument to determine a more accurate estimate and possibly predict the dependence on the energy (or, equivalently, the temperature). Our numerical analysis indicates that the largest LE stays indeed positive in the ordered phase. Possibly, it can remain positive in the limit  $U \rightarrow 0$ , but a

purely numerical approach is out of question because one would need to simulate large enough systems to guarantee the presence of some oscillators near the saddle of the corresponding potential. Near  $U = 0$ , the probability for an oscillator to come close to the separatrix goes to zero, and thus simulations are utterly unfeasible.

Although we have not been able to extend the theoretical arguments beyond the largest exponent, we have undertaken also a general investigation of the entire Lyapunov spectrum to investigate the extensivity of the chaotic dynamics. Our numerical analysis suggests that the asymptotic number of unstable directions is not extensive (it grows probably like  $\ln N$ ). It would be desirable to develop some even approximate argument to justify this scaling behavior, which is, so far, only based on numerical simulations.

Finally, we have also analyzed the Lyapunov spectrum for the 2D HMF. Such a system is less pathologic than the 1D model, since the single oscillator dynamics is chaotic and it is therefore obvious to expect positive LEs. However, a problem remains to be settled regarding the scaling behavior of the full spectrum. On the basis of all arguments developed here and in Ref. [15], we would expect that the bulk of the Lyapunov spectrum (at least for  $r < 1$ ) converges to a finite value. However this is not yet seen in our simulations. We cannot exclude that this is because the finite value associated to the single oscillator dynamics is really small.

All in all, the results presented here need to be put of firmer ground by more rigorous mathematical approaches, especially since we have shown that strong finite-size effects are at play. The open questions mentioned above also require further work. It is our hope that the rather subtle phenomena uncovered here will attract such needed attention in the future.

## Acknowledgments

We thank M. Antoni for providing us the figure of the phase diagram of the generalized HMF model and S. Ruffo for useful discussions. AT thanks X. Leoncini for fruitful exchanges of information.

- 
- [1] M. Antoni and S. Ruffo, Phys. Rev. E **52**, 2361 (1995).
  - [2] T. Dauxois, V. Latora, A. Rapisarda, S. Ruffo, and A. Torcini, in *Dynamics and Thermodynamics of Systems with Long Range Interactions*, eds: T. Dauxois *et al.*, Lecture Notes in Physics, vol. 602 (Springer, Berlin, 2002), p. 458.
  - [3] A. Campa, T. Dauxois, and S. Ruffo, Phys. Rep. **480**, 57 (2009).
  - [4] V. Latora, A. Rapisarda, and S. Ruffo, Phys. Rev. Lett. **80**, 692 (1998); Physica D **131**, 38 (1999).
  - [5] A. Crisanti, G. Paladin, and A. Vulpiani, *Products of*  
*Random Matrices in Statistical Physics* (Springer-Verlag, Berlin, 1993).
  - [6] C. Anteneodo and R. O. Vallejos, Phys. Rev. E **65**, 016210 (2001).
  - [7] M.-C. Firpo, Phys. Rev. E **57**, 6599 (1998).
  - [8] T. Manos and S. Ruffo, arXiv:1006.5341 (2010), to appear in *Transport Theory and Statistical Physics*.
  - [9] S. Tănase-Nicola and J. Kurchan, J. Phys. A: Math. Gen. **36**, 10299 (2003).
  - [10] H. Daido, Prog. Theor. Phys. Suppl. **79**, 75 (1984); Prog. Theor. Phys. **72**, 853 (1984).

- [11] R. Livi, A. Politi, and S. Ruffo, J. Phys. A **25**, 853 (1992).
- [12] A. Torcini, R. Livi, A. Politi, and S. Ruffo, Phys. Rev. Lett. **78**, 1391 (1997).
- [13] F. Cecconi and A. Politi, Phys. Rev. E **56**, 4998 (1997).
- [14] R. Zillmer, V. Ahlers, and A. Pikovsky, Phys. Rev. E **61**, 332 (2000).
- [15] K. A. Takeuchi, H. Chaté, F. Ginelli, A. Politi, and A. Torcini, Phys. Rev. Lett. **107**, 124101 (2011).
- [16] M. Antoni, S. Ruffo, and A. Torcini, Phys. Rev. E **66**, 025103 (2002).
- [17] M. Antoni and A. Torcini, Phys. Rev. E **57**, R6233 (1998); A. Torcini and M. Antoni, Phys. Rev. E **59**, 2746 (1999).
- [18] Y. Kuramoto, *Chemical oscillations, waves, and turbulence* (Dover Publishing, 2003, New York).
- [19] R. I. McLachlan and P. Atela, Nonlinearity **5**, 541 (1992).
- [20] In the following, we occasionally refer to the absolute scale,  $h_i = p_i^2/2 + 1 - M \cos(\theta_i - \phi)$ , wherever it is more convenient.
- [21] Throughout this paper we will write the explicit subscript  $(\cdot)_N$  when we wish to stress the finite size effects of the global magnetization.
- [22] H. Daido, J. Stat. Phys. **60**, 753 (1990).
- [23] A. Pikovsky and S. Ruffo, Phys. Rev. E **59**, 1633 (1999).
- [24] H. Hong, H. Chaté, H. Park, and L.-H. Tang, Phys. Rev. Lett. **99**, 184101 (2007).
- [25] This can be derived from  $U = \frac{1}{Z} \int dp \int d\theta [\frac{p^2}{2} + \frac{1}{2}(1 - M \cos \theta)] e^{-\beta \mathcal{H}}$  in the same way as for the self-consistency equation (11).
- [26] C. Kittel and H. Shore, Phys. Rev. **138**, A1165 (1965).
- [27] R. Botet, R. Jullien, and P. Pfeuty, Phys. Rev. Lett. **49**, 478 (1982).
- [28] I. Shimada and T. Nagashima, Prog. Theor. Phys. **61**, 1605 (1979); G. Benettin, L. Galgani, A. Giorgilli and J. M. Strelcyn, Meccanica **15**, 21 (1980).
- [29] We have verified that our results do not depend on the choice of the time interval  $\tau$  as long as it is of order  $\mathcal{O}(1)$ .
- [30] F. Ginelli, P. Poggi, A. Turchi, H. Chaté, R. Livi, and A. Politi, Phys. Rev. Lett. **99**, 130601 (2007).
- [31] K. A. Takeuchi, F. Ginelli, and H. Chaté, Phys. Rev. Lett. **103**, 154103 (2009).
- [32] H.-l. Yang, K. A. Takeuchi, F. Ginelli, H. Chaté, and G. Radons, Phys. Rev. Lett. **102**, 074102 (2009); K. A. Takeuchi, H.-l. Yang, F. Ginelli, G. Radons, and H. Chaté, arXiv:1107.2567 (2011).
- [33] A. D. Mirlin, Phys. Rep. **326**, 259 (2000).
- [34] G. Parisi and A. Vulpiani, J. Phys. A **19**, L425 (1986).
- [35] Strictly, this estimate of the metric entropy is only an lower bound, because the binary symbolic representation is not necessarily the optimal choice.